

Evaluation of novel nanocomposites for enhanced anticancer activity of XLasp-P2 peptide

Yasuri Amarasekara^{a,b,d}, Inoka C. Perera^c, Nuwanthi P. Katuwavila^{a,d}, Ranga S. Jayakody^b, Gehan A.J. Amaratunga^{a,e}, Laksiri Weerasinghe^{a,b,*}

^a Sri Lanka Institute of Nanotechnology (SLINTEC) / SLINTEC Academy, Mahenwatta, Pitipana, Homagama, Sri Lanka

^b Department of Chemistry, Faculty of Applied Sciences, University of Sri Jayawardenapura, Gangodawila, Nugegoda, Sri Lanka

^c Department of Zoology and Environment Sciences, Faculty of Science, University of Colombo, Colombo, Sri Lanka

^d Department of Biomedical Science, Faculty of Science, NSBM Green University, Mahenwatta, Pitipana, Homagama, Sri Lanka

^e Electrical Engineering Division, Department of Engineering, University of Cambridge, 9 JJ.Thomson, Avenue, Cambridge CB3 0FA, UK



ARTICLE INFO

Article history:

Received 3 September 2021

Revised 4 February 2022

Accepted 9 February 2022

Available online 11 February 2022

Keywords:

XLaspP2-RA

AMP

SPPS

RD cells

Graphene oxide

APTES modified HNTs

ABSTRACT

A nanotechnology based approach to improve the anticancer activity of XLaspP2-RA, against muscle rhabdomyosarcoma (RD) is reported. The XLaspP2-RA was successfully synthesized, and the structure was confirmed by ¹H NMR spectroscopy. Loading of XLaspP2-RA into APTES modified halloysite nanotubes and Graphene Oxide were confirmed by FT-IR spectroscopy. The encapsulation efficiency of 97% and a loading capacity of 4% are obtained for the optimized formulation of the XLaspP2-RA-fHNT composite. For the XLaspP2-RA-GO composite, the values are 85% and 7%, respectively. The dialysis method investigated the release kinetics of XLaspP2-RA from both composites, showing an initial burst release followed by a controlled release over 24 h period. Both systems' *in vitro* release profiles were fitted more closely with the Higuchi square root model. The improved enzymatic stability was seen with a half-life extension to 11–14 h in both nanocomposites. An enhanced *in vitro* cytotoxicity against RD cells with XLaspP2-RA loaded fHNT was observed with having an IC₅₀ value of 3.57 ± 0.07 µg/mL while it was 15.46 ± 0.18 µg/mL with GO loaded composite. The results show the potential of developing XLaspP2-RA as a novel therapeutic for Muscle rhabdomyosarcoma with an fHNT based nano-formulation strategy.

© 2022 Elsevier B.V. All rights reserved.

1. Introduction

With 200 years of ongoing research, cancer is still remains as one of the most complex multifactorial diseases in the world. According to the new global cancer estimation, the worldwide cancer cases have increased to 19.3 million, with 10 million deaths in 2020, and is projected to rise to 26 million by 2040 [1,2]. At present, chemotherapy is considered as the preferred cancer treatment method in medical oncology. The inherent side effects of common chemotherapy drugs, especially on fast-growing healthy cells and immunity systems, have redirected the focus of oncology towards novel molecular methods such as targeted drug therapy as an emerging new strategy [3].

Antimicrobial peptides (AMPs) with 2–50 amino acids have been identified as an alternative resource for small molecular drug discovery. Despite their essential roles in innate immunity [4], the

ability of tissue penetration and efficient uptake into heterogeneous cancer cells have proven these molecules as a resourceful alternative in anticancer drug discovery [5]. In addition to high specificity and efficient tumour penetrating ability, anticancer peptides (ACPs) derived from AMPs have a remarkable ability in differentiating the cell membranes of malignant cells from normal cell membranes [6,5]. There has been an alleviating interest in ACPs derived from natural sources or *in silico* methods in anticancer drug discovery in recent years. Magainin II is an antimicrobial peptide, originally isolated from the skin of the African clawed frog, *Xenopus laevis* [7]. Based on the *in vitro* studies, magainin II exhibit anticancer activity against melanomas, breast cancer, lung cancer, and bladder cancers [8,9]. Furthermore, aurein 1.2, an isolated AMP from the frog *Litoria aurea* [10], and Dermaseptin-PH, isolated from the frog called *Pithecopus (Phyllomedusa) hypochondrialisan* [11], have been reported for their anticancer activities against various cancer cell lines, including MCF-7, U251MG, H157, and PC-3 [12]. Due to the enhanced efficacy in anticancer activity, few peptides have already advanced into the clinical trials, including the AMP-derived LTX-315 and LL-37 as treatments for melanoma and solid tumours [13].

* Corresponding author at: Sri Lanka Institute of Nanotechnology (SLINTEC) / SLINTEC Academy, Mahenwatta, Pitipana, Homagama, Sri Lanka.

E-mail address: laksiri@sjp.ac.lk (L. Weerasinghe).

It is worthy to note that even with enhanced therapeutic effects, the inherent undesirable physicochemical properties of peptides such as variable solubility, low bioavailability, limited stability, and difficulties in systemic delivery hinder their therapeutic applications [14]. The limited stability of peptides is mainly due to rapid digestion by proteolytic enzymes in the digestive system and plasma [15,16]. Therefore, developing new strategies to address these issues has become a significant focus. Thus, nano-based drug delivery systems have been developed to deliver therapeutic molecules like peptides, proteins, DNA, and aptamers into malignant cells [17]. Nanomaterials offer enhanced permeability and retention (EPR) effect due to various chemical and physical properties, thereby sparing the normal healthy tissues [18]. Moreover, along with the tuneable properties like size, shape, and surface charge, nanomaterials release the active compounds in a controlled manner while improving the drugs' solubility and stability [18,19].

In this study, a peptide analogue (EDLDED) was designed based on a novel AMP, XLAsp-P2 (DEDLDE). This natural peptide was initially isolated from the skin tissues of *Xenopus laevis* has been reported to exhibit moderate antibacterial activity [20]. The analogue sequence was designed based on the retro analogue concept, whereas reversing the sequence of the template peptide by keeping the exact configuration of chiral centres but an opposite rank order of amino acid residues [21]. Further, our *in silico* studies, including docking and (un)binding simulation analyses to identify XLAspP2-RA interacting residues of human Akt-1 receptor, have provided some interesting insights on XLAspP2-RA's capability as an allosteric inhibitor of Akt-1 and its inhibitory mechanism [22].

On this note, we aimed to explore the potential of using hybrid nanomaterials such as graphene oxide (GO) [23–25] and natural halloysite nanotubes (HNTs) [26] as scaffolds for peptide conjugation to resolve some of the remaining issues in peptide-based drug delivery while evaluating the anticancer activity of XLAsp-P2 analogue against rhabdomyosarcoma.

2. Materials and methods

2.1. Solid phase synthesis of XLAspP2-RA peptide

N α -9-fluorenylmethyloxycarbonyl (Fmoc) amino acids, Wang resin, were purchased from AAPPTec, USA and the remaining chemicals and reagents including Trifluoroacetic acid (TFA), N,N-Dimethylformamide (DMF), N,N-Diisopropylethylamine (DIPEA), 1-Hydroxybenzotriazole (HOBt), 2-(1H-Benzotriazole-1-yl)-N,N,N',N'-tetramethylammonium tetrafluoroborate (HBTU), Dichloromethane (DCM), Piperidine, N,N'-dicyclohexylcarbodiimide (DCC), diisopropyl carbodiimide (DIC), Acetic anhydride, Methanol, 95% isopropanol, Potassium chloride, Phenol, Magnesium sulfate, Glacial acetic acid, Acetonitrile, Potassium cyanide, Ninhydrine, Pyridine, Ether, and Triisopropylsilane (TIPS), MTT (3-(4,5-dimethyl thiazol-2-yl)-2,5-diphenyl tetrazolium bromide), DMSO, FBS, DMEM, cycloheximide, and PBS were purchased from Sigma-Aldrich, USA. HPLC grade solvents were used for the synthesis and purification steps.

2.1.1. Synthesis

XLAsp-P2 analog was synthesized according to the standard solid-phase peptide synthesis (SPPS) protocol using Wang resin with 1.1 mmol/g loading capacity. The amino-acid residues were coupled using HOBt/HBTU/DIPEA (1:1:1) for 3 h. N-terminal Fmoc group was removed using piperidine prior to each amino acid coupling. Finally, the peptide was removed from the resin by treatment with TFA/DCM/TIPS (5:4:1). The synthesis was repeated on a 1–5 mmol scale using the same SPPS protocol. Further, large-scale synthesis was carried out using Discovery 4 Multiple Peptide Synthesizer (Peptide Machines, Inc., USA) according to standard single

coupling protocol. After cleavage, the crude peptide was precipitated with cold anhydrous diethyl ether and stored at 4 °C until further purification.

2.1.2. HPLC analysis and purification

Crude XLAspP2-RA was analyzed using analytical HPLC (Shimadzu, Japan) using a reverse-phase C-18 column (4.6 × 250 mm, 5 μ m). The peptide was eluted in 0.05% TFA in water for 15 min at a 1 mL/min flow rate with detection at 215 nm. The purification was done using a preparative HPLC system (LC-20AP, Shimadzu, Japan) on a C18 column (25 mm × 250 mm). The peptide was eluted with 0.05% TFA in the water at a 10 mL/min flow rate with detection at 220 nm. Fractions from multiple runs at the peak of t_R 7.05 min were collected and combined. The purified peptide was freeze-dried and stored at –20 °C.

2.1.3. Characterization of XLAspP2-RA

The chemical structure of the peptide was confirmed by Nuclear magnetic resonance (¹H NMR) spectroscopy. ¹H NMR was performed on a Bruker Ascend™ 400 MHz NMR Spectrometer in D₂O at 25 °C. Chemical shifts were measured with reference to tetramethylsilane (TMS). The pure peptide was further analyzed by MS using a direct injection apparatus equipped with a Single Quadrupole Detector (SQD2) (Waters, USA) at 25 °C. All spectra were plotted as total ion current (TIC) versus time and given the supporting information (Figs. S1–S3).

2.2. Synthesis of peptide composites

2.2.1. Synthesis of f-HNT-peptide composite

The surface modification of HNT by grafting 3-aminopropyl triethoxysilane (APTES, H₂NCH₂CH₂CH₂Si-(OCH₂CH₃)₃) was carried using a reported method [27]. The f-HNT-XLAspP2-RA hybrid was prepared by mixing peptide and f-HNTs in 1:1 (w/w) in 1 mL of CH₃CN/H₂O (5%). The mixture was stirred at room temperature for 24 h. The reaction mixture was centrifuged, and the resulting solid precipitate was washed several times with distilled water. The supernatant was analysed by analytical HPLC to confirm the encapsulation [28,29]. The product obtained was oven-dried and stored in the dark until further use.

2.2.2. Synthesis of GO-peptide composite

GO was prepared by a modified Hummer's method starting from Sri Lankan vein graphite (purity ~99%) [30]. The composite was synthesized by mixing XLAspP2-RA and GO in 1:1 (w/w) in 1 mL of CH₃CN/H₂O (5%). The mixture was stirred at room temperature for 24 h and purified by centrifugation at 10,000 rpm for 15 min. After several washing steps, the pH was adjusted to 7. The product was oven-dried before further use and storage. The supernatants obtained during the previous washing steps were separated and analysed using HPLC. Loading and encapsulating efficiencies were calculated as described in 2.2.4.

2.2.3. Characterization of the composites

Fourier Transform Infrared (FTIR) measurements of composites were carried out using a Bruker Vertex 80 IR spectrometer (Germany) at a resolution of 4 cm⁻¹ from 4000 to 400 cm⁻¹. Ultraviolet-visible (UV-VIS) spectra were recorded using a UV-3600 (Shimadzu, UV-VIS-NIR, Japan).

2.2.4. Determination of encapsulation efficiency and loading capacity

The amount of incorporated peptide in the composite was determined by measuring the UV absorbance of the supernatant at 264 nm (S4). The weight was calculated from a calibration plot obtained for different concentrations of a standard peptide solution.

Percentage encapsulation efficiency (% EE) and loading capacity (% LD) was calculated using the following equations:

$$\% \text{ Encapsulation efficiency (EE)} = \frac{m1 - m2}{m1} \times 100\%$$

$$\% \text{ Loading capacity (LD)} = \frac{m1 - m2}{m} \times 100\%$$

Where, $m1$ = initial weight of the peptide, $m2$ = remaining weight of the peptide in the supernatant, and m = weight of the final composite.

2.3. Release kinetics of XLAsp-P2 analog

The release characteristics of the peptide from the composites were studied in phosphate-buffered saline solution -PBS (pH 7.4). Centrifuged composites were dispersed in 5 mL of release medium, trapped inside a dialysis membrane (3500 MWCO), and immersed in 25.0 mL of the release medium. The setup temperature was maintained at 37 °C in the dark with mild agitation. At pre-set time points, 3.00 mL aliquots were withdrawn, and the peptide concentration was determined using UV spectrometry. After each withdrawal, the medium was replaced with 3.00 mL of fresh medium. All measurements were performed in triplicates.

The peptide release kinetics was analysed using the following mathematical models: zero-order kinetic, first-order kinetic, Higuchi equation [31], Korsmeyer-Peppas equation [32] and Hixson-Crowell model [33].

2.4. Assessment of proteolytic stability

The stability of the peptides was tested using a reported procedure with slight modifications [34]. In brief, a peptide stock solution (10 mg/mL) was incubated with 10% PBS at 37 °C. At various time points (0-24 h), 200 µL aliquots were withdrawn, mixed with CH₃CN, and further mixed by vortexing, and incubated at 37 °C for 5 min to terminate the enzyme degradation. The final mixture was centrifuged at 10,000 rpm, 10 min, and then the supernatant was withdrawn and immediately analysed by UV-VIS.

2.5. In vitro cytotoxicity of peptide and its composites

The cellular cytotoxicity of the test materials was determined using an MTT (3-(4,5-dimethyl thiazol-2-yl)-2,5-diphenyl tetrazolium bromide) assay as previously described [35]. The rhabdomyosarcoma (RD ATCC® CCL-136™) and Vero cells (ATCC® CCL-81™) were seeded in 24-well plates at a density of 2×10^5 cells per well followed by incubation for 24 h at 37 °C. After the incubation period, confluent monolayers were exposed to different concentrations of test materials for further 24 h incubation at 37 °C. In all experiments, 50 µL of cycloheximide (5 mM) was used as the positive control, and negative control contained the growth media and the solvent mixture used to dissolve the test compound. The blank was used during the calculation, consisting of the growth medium without cells, MTT, and solubilizing buffer. At the end of this incubation period, cells were washed with phosphate-buffered saline (PBS) solution, and MTT assay was performed as described below. The PBS washed wells were introduced with 200 µL of a working solution that contains 0.5 mg/mL MTT in a complete medium. The cells were incubated at 37 °C for 3 h, and the growth medium was removed carefully. The remaining formazan crystals were solubilized in 100 µL of DMSO, and absorbance was measured at 570 nm. Percentage cell viability was determined using the formula. [36] Negative control was considered as having 100% viability.

$$\text{Percentage Viability} = \frac{A_{\text{treatment}} - A_{\text{blank}}}{A_{\text{control}} - A_{\text{blank}}} \times 100\%; A = \text{absorbance}$$

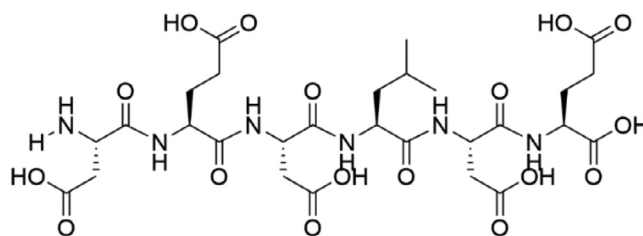


Fig. 1. Structure of XLAsp-P2 retro analog.

2.6. Statistical analysis

The linearity of the release kinetic models was studied using the linear regression analysis based on the least-squares regression method. The standard deviation (SD) and the correlation coefficient (R^2) were used to determine the fitting kinetic model. IC_{50} values were determined by non-linear regression analysis ($R^2 > 0.95$) of the corresponding dose-response curves of percentage inhibition of cell viability and concentration of the test solutions. Experiments were performed in triplicate, and the values given represent three independent experiments using Origin Pro version 8.0 (OriginLab Corporation, Northampton, MA, USA) or GraphPad Prism version 7.0 (GraphPad Software, La Jolla, CA, USA). All results were expressed as mean \pm SD.

3. Results and discussion

3.1. Synthesis and characterization

As described below, the novel antimicrobial peptide analog of XLAsp-P2 was successfully synthesized in good yield (76.4%). Their predicted molecular mass was confirmed using mass spectrometry. Predicted molecular mass ($M+H$)⁺ showed molecular ion peak m/z at 735.31 (calcd 734.26) (Fig. S2). ¹H NMR Data obtained for analog was also consistent with the structural assignment and the following peaks were observed: NMR (400 MHz, in D₂O, 25 °C) δ 4.47 – 4.31 (m, 2H), 4.10 (t, $J = 6.5$ Hz, 1H), 3.58 (q, $J = 7.1$ Hz, 1H), 3.36 (s, 3H), 3.07 – 2.77 (m, 6H), 2.58 – 2.41 (m, 3H), 2.10 – 1.98 (m, 3H), 2.06 – 1.92 (m, 1H), 1.65 – 1.43 (m, 3H), 1.39 – 1.31 (m, 1H), 1.19 (t, $J = 7.1$ Hz, 2H), 0.91 – 0.73 (m, 6H) (Fig. S3). The spectral data are in good agreement with naturally extracted XLAsp-P2, which was previously reported by Zhang et al. [20]. Hence, the interpretation of spectral data convincingly proved the identity of the retro analog of the peptide (Fig. 1).

3.2. Synthesis of peptide composites

To improve the stability of the peptide, the purified peptide was encapsulated with functionalized HNT (fHNT) and GO to form composites.

3.2.1. Synthesis of f-HNT-peptide composite

The amino functionalization of the halloysite nanotubes with an organosilane. (3-aminopropyl) triethoxysilane (APTES) was achieved. APTES based amino functionalization is a well-known synthetic method due to its ease of usage and low toxicity. APTES's ability to form silyl ethers with the hydroxyl groups on the HNT surface is the basis of this functionalization. As shown in the FT-IR spectrum in Fig. 2A, the peaks at 3624 and 3695 cm^{-1} correspond with the stretching vibrations of the interlayer and superficial hydroxyl groups. FTIR peaks at 2924 and 1492 cm^{-1} are diagnostic peaks for the stretching and bending vibrations of CH₂ groups in amino-modified HNT. The deformation -SiCH vibration at 1328 cm^{-1} , and the deformation -NH₂ vibration at 1558 cm^{-1}

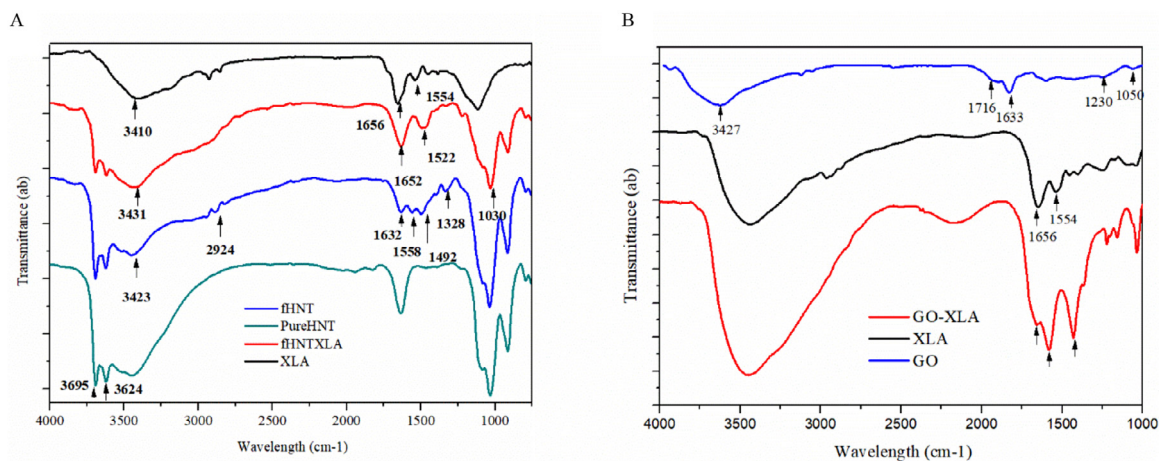


Fig. 2. FTIR spectra: A. Synthesized HNT composite B. GO composite.

was also evident in the spectrum [27,37]. Successful incorporation of peptide with fHNT surface was also confirmed by FTIR spectroscopy. The peaks at 3431 cm⁻¹ could be ascribed to the stretching vibrations of hydroxyl groups. Characteristic bands for O–Si–O were observed around 1030 cm⁻¹. The prominent absorption peaks confirmed the peptide incorporation in the composite at 1522 and 1652 cm⁻¹, which corresponded to the stretching frequency of the C=O of the amide groups. Due to potential H-bond formation, amino functionalization could enhance the peptide-fHNT interactions (Fig. 2A). Further, this NH₂-modified fHNT demonstrated a much higher loading capacity, which also agrees with the previous reports [38,39]. This could be due to enhanced electrostatic interaction between the carboxyl group of the peptide and the –NH₂ group present in the functionalized nanotubes [40,41].

3.2.2. Synthesis of GO-peptide composite

The formation of the GO-peptide nanocomposite was confirmed by the FTIR spectra (Fig. 2B). The characteristic peaks at 3427 cm⁻¹, 1716 cm⁻¹, 1633 cm⁻¹, 1230 cm⁻¹, and 1050 cm⁻¹ in the GO spectrum were due to –OH stretching, C = O stretching, aromatic C = C stretching, epoxy C–O stretching, and alkoxy C–O stretching vibrations. The existence of peptides in the GO-XLA conjugates is supported by the presence of amide bonds from the backbone of the peptide at 1639 cm⁻¹ and 1567 cm⁻¹ [42,43].

The loading of peptides on GO occurs through non-covalent interactions [44,45]. Incubation time and the optimized peptide: GO ratio are the major determining factors in controlling the peptide encapsulation with GO substrate [46]. It has been reported that peptide can also interact with GO substrate via electrostatic interactions [47,48]. Hydroxyl, epoxide, carbonyl, and carboxylic acid groups also can contribute to the formation of covalent and non-covalent bonds with the peptide (Fig. 2B) [49,50].

3.3. Drug loading and in vitro release of XLAspP2-RA peptide

The presence of the peptide in the composite was confirmed and quantified in terms of peptide loading efficacy. The encapsulation efficiency of the functionalized GO- XLAspP2-RA composite was 85%, and the loading capacity was 7%. In peptide-fHNT composite, encapsulation efficiency was 97%, while drug loading capacity was 4%.

Drug releasing kinetics is an essential aspect of a drug delivery mechanism. The release profiles of the peptide composites were conducted in PBS solution using a direct dispersion method. The obtained cumulative release profile for both composites is pre-

Table 1

The correlation coefficient (R²) of different kinetic models for peptide release.

Model name	R ² (XLAspP2-RA-fHNT)	R ² (XLAspP2-RA-GO)
Zero-order model	0.9685	0.9526
First-order model	0.974	0.9606
Higuchi model	0.9972	0.986
Korsmeyer-Peppas model	0.9828	0.9824
Hixson-Crowell model	0.9672	0.952

sented in Fig. 3. The cumulative release values of the peptide from the XLAspP2-RA-fHNT and XLAspP2-RA-GO membranes were achieved by 86%, 73% within 24 h, respectively.

The release profiles of the peptide-composites showed an initial faster release followed by a slower release for all tested composite materials, with equilibrium established after a time period approaching 1500 mins. Considering the higher release rate observed in the fHNT- XLAspP2-RA composite, the initial burst release of the peptide could result from the rapid dissolution of the peptide from the outer surface of the functionalized nanotube. Subsequently, the incorporated peptide inside the pores of the nanotube is released in a sustained manner within a period of 24 h at pH 7.4 [51]. This releasing pattern is also in line with the previously reported work [52]. Based on our results, the slow release of the peptide from the composite can increase its bioavailability. This is further confirmed by the cytotoxicity results obtained later in the investigation. As reported in Kumeria et al., 2013 more than 85% of hydrogen bond-forming groups in GO are deprotonated (e.g., CO₂) at pH 7.4 [53]. Therefore, most H-bonding groups on the GO surface exist as negatively charged entities leading to a weak interaction between the negatively charged peptide and the GO composite. This could lead to significantly lower encapsulation capacity and faster release [53].

In addition to these initial releasing experiments, the *in vitro* release kinetics were evaluated by fitting the drug release data with the five kinetic models. The model corresponding with the highest correlation coefficient value (R²) was selected as the best model to describe obtained drug release kinetics. The calculated R² values for the chosen composites are represented in Table 1. The Higuchi square root model showed the highest R² value. At the same time, the release mechanism of peptide-loaded composites were fitted to

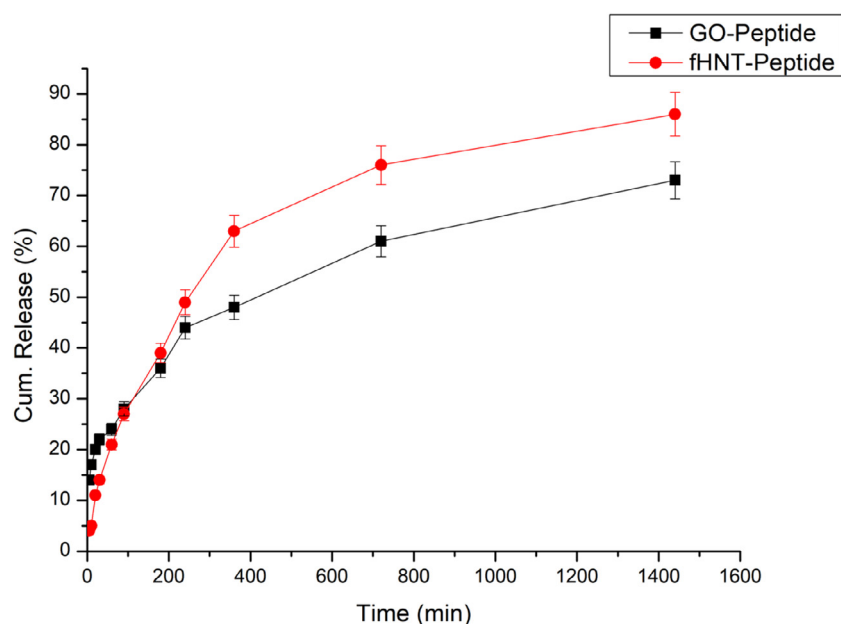


Fig. 3. Cumulative release of peptide at preselected time intervals in pH 7.4 buffer. Results were reported as mean \pm SD, $n = 3$.

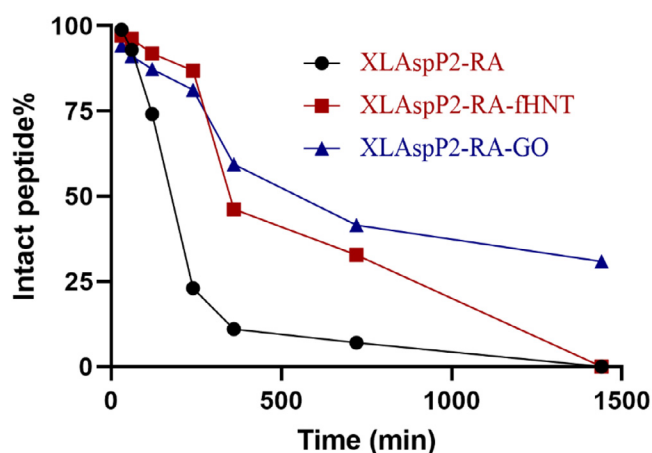


Fig. 4. Peptide stability in FBS at 37 °C.

the Fickian diffusion with exponent $n = 0.49$ for fHNT composite and $n = 0.51$ for GO composite.

Further, the drug release was found to be best fitted by the Higuchi square root model ($R^2 = 0.9972$ for XLAspP2-RA-fHNT and $R^2 = 0.986$ for XLAspP2-RA-GO), which implies that release of drug as a square root of time-dependent process and diffusion controlled [54]. The Higuchi model states the rate of diffusion of the test material from a matrix where the drug loading exceeds its solubility in the matrix into a surrounding fluid [55]. Since the primary mechanism of peptide release is diffusion controlled from Higuchi, diffusion mechanisms were confirmed by fitting the release data to the empirical equation proposed by Korsmeyer and Peppas [32]. Fick's law of diffusion governs the rate of release of the peptide into the surrounding fluid. According to Fick's law, the peptide-loaded into the matrix is released by diffusion transport in a gradual and steady manner. This explains the initial burst and the gradual release observed at the initial and later stages of the release, respectively [56,57].

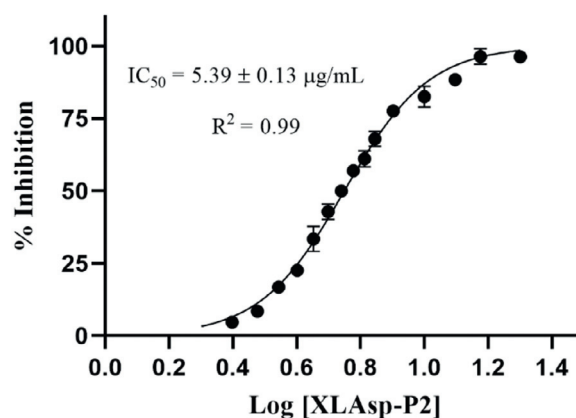


Fig. 5. The percentage inhibition. The viability of the RD cell line was determined by MTT assay after 24 h treatment with the XLAspP2-RA peptide. The graphical data represent as mean \pm SD of three independent experiments ($n = 3$).

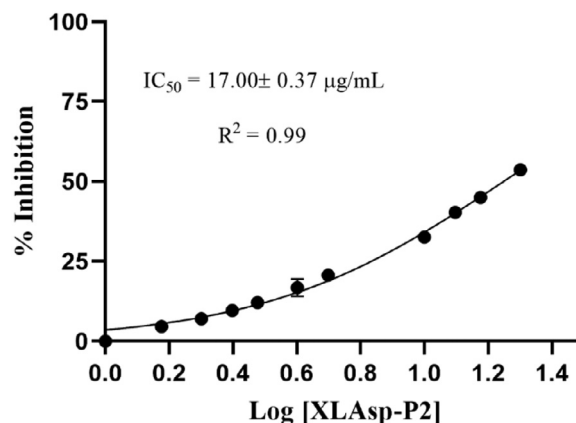


Fig. 6. The percentage inhibition. Viability of Vero cell line as determined by MTT assay, after 24 h treatment with the XLAspP2-RA peptide. The graphical data are represented as mean \pm SD of three independent experiments ($n = 3$).

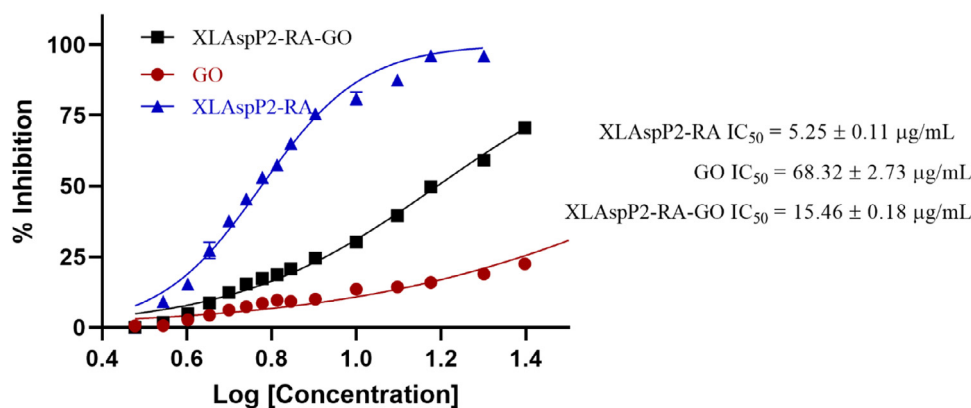


Fig. 7. The percentage inhibition of peptide-loaded composites. GO and GO- XLAspP2-RA on RD cell line as determined by MTT assay, after 24 h treatment. The graphical data are represented as mean ± SD of three independent experiments ($n = 3$).

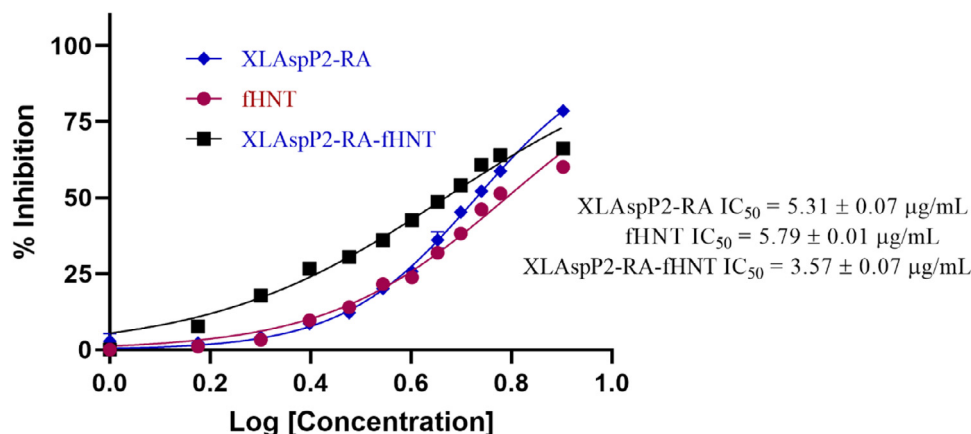


Fig. 8. The percentage inhibition of peptide-loaded composites. fHNT and fHNT- XLAspP2-RA on RD cell line as determined by MTT assay, after 24 h treatment. The graphical data are represented as mean ± SD of three independent experiments ($n = 3$).

3.4. Enzymatic stability of XLAspP2-RA

Peptide stability was tested using an assay incorporating FBS. The half-life of degradation of the peptide was observed to be 4–5 h. Encapsulation with fHNT and GO enhanced the stability, extending the half-life to 11–14 h (Fig. 4). It was further observed that 42% of peptides in the GO composites remained in the solution after 12 h incubation and the amount of peptide remained in the fHNT composite was 33%.

Peptide-based therapeutic drugs are exposed to a wide range of proteases *in vivo*. Upon proteases degradation, the resulting short and typically hydrophilic peptide segments are cleared effectively by renal excretion. Among the different methods for improving proteolytic stability, encapsulation in nanomaterials is a viable strategy in targeted drug delivery [58,59].

Based on our observations, the half-life of XLAspP2-RA peptide in serum has increased from 5 h to 11 h and more than 14 h upon encapsulating with fHNT and GO, respectively. The higher stability of the composites may also influence the efficacy measured in the stability assay as well as *in vitro* cytotoxicity assay [60].

3.5. Induced in-vitro cytotoxicity activity

An MTT assay was carried out on the RD cell line to investigate the potential anticancer effect of peptide-loaded composites. A dose-dependent increase in percentage inhibition of cell viability over a concentration range of 1.5–8.0 μg/mL of XLAspP2-RA against the RD cell line was observed (Fig. 5). The maximum of 78.8%

cell growth inhibition was observed at 8.0 μg/mL of the test solution. The peptide itself exhibited a strong cytotoxic effect against RD cells by showing an IC₅₀ (the concentration of drug at which cell viability was reduced by 50% compared to untreated cells) of 5.39 ± 0.13 μg/mL in a dose-dependent manner. In contrast, positive control (cycloheximide) exhibited 79.8% growth inhibition at a concentration of 5 mM.

The IC₅₀ value obtained for the peptide against a normal mammalian cell line (Vero: kidney epithelial cells from a monkey) was 17.00 ± 0.37 μg/mL (Fig. 6). RD cells and Vero cells were treated with GO-XLAspP2 and fHNT- XLAspP2-RA compounds at different concentrations for 24 h. The obtained IC₅₀ values are mentioned in Table 2. GO exhibited relatively high viability towards RD cells. Even at a very high concentration (100 μg/mL), the viability of RD cells remained 64.59%. In the absence of the peptide, the cell viability of the GO treated cells remained above 80%, which indicated that the cytotoxicity of GO- XLAspP2-RA composite was attributed to the peptide (Fig. 7). After 24 h incubation, fHNT- XLAspP2-RA composite fHNTs exerted relatively low growth-inhibitory cell activity up to 6 μg/mL, indicating the high level of biocompatibility of halloysite nanotubes (Fig. 8).

The cytotoxic property of the compounds was investigated through morphological changes on the RD cell line and Vero cell line using an inverted phase-contrast microscope. Figs. 9 and 10 show that the control (untreated) cells maintained their original morphology and were mostly attached to the plate. But, treated with peptide composites exhibited morphological variations on the cells after 24 h. Typical apoptotic features such as membrane blebbing, change in the shapes of the cells, and loss of contact with ad-

Table 2
IC₅₀ values (µg/mL) of each composite obtained after 24 incubations.

Composite type	XLAspP2-RA	GO	XLAspP2-RA-GO	fHNT	XLAspP2-RA-fHNT
IC ₅₀ µg/mL	5.39 ± 0.13	68.32 ± 2.73	15.46 ± 0.18	5.79 ± 0.10	3.57 ± 0.07

Each value is a mean of 3 separate experiments.

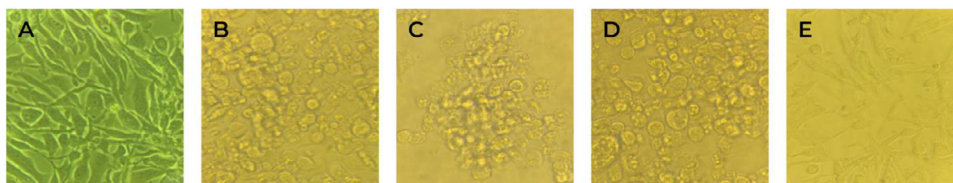


Fig. 9. Light micrographs of RD cell line after 24 h of incubation at different concentrations ($\times 40$). (A) Negative control; (B) Cycloheximide as the positive control (5 mM, 50 μ L, 79.83% inhibition); (C) XLAspP2-RA (6 μ g/mL, 59.29% inhibition); (D) fHNT-XLA (6 μ g/mL, 70.5% inhibition); (E) GO-XLA (6 μ g/mL, 19.88% inhibition).

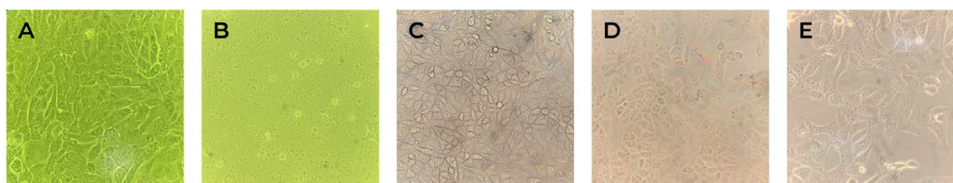


Fig. 10. Light micrographs of Vero cell line after 24 h of incubation at different concentrations ($\times 40$). (A) Negative control; (B) Cycloheximide as the positive control (5 mM, 50 μ L, 88.79% inhibition); (C) XLAspP2-RA (6 μ g/mL, 14.94% inhibition); (D) fHNT-XLA (6 μ g/mL, 12.85% inhibition); (E) GO-XLA (6 μ g/mL, 9.07% inhibition).

adjacent cells were observed; the number of cells was also decreased [61]. This suggests that the peptide has the potential for *in vivo* anticancer applications. In evaluating the effect of the peptide on circulating blood cells, a preliminary study conducted by Zhang et al., 2017 has obtained a low haemolytic activity at 64 μ M [20]. In this study, the synthesised peptide exhibited a potent antiproliferative effect on cultured rhabdomyosarcoma cells (ATCC® CCL-136™) in a dose-dependent manner, according to the typical forms of morphological changes which occur in the cells at the early stages of apoptosis. Furthermore, the predicted selectivity index shown by the peptide against RD cells was 3.15, indicating less cytotoxic effects on normal cells [36,62,63].

In addition to the enhanced cytotoxicity of XLAspP2-RA peptide, the increased efficacy against RD cells in fHNT composite form was also evident. The induced cytotoxicity effect allows the use of relatively low concentrations of peptides to achieve a significantly higher anticancer activity *in vitro*. This nanomaterial-peptide-based composite reported enables an effective apoptosis-mediated anticancer effect with lower potential side effects while using a minimal effective dose. The underlying mechanism of XLAspP2-RA induced cell death is under investigation using a multidisciplinary approach that employs computational chemistry and cell biology.

4. Conclusion

Natural AMPs are unique molecular structures with promising biological activities that can be further harnessed as potential treatments for existing therapeutic problems such as cancer. Many studies have focused on the biological activities of peptides. However, there are challenges associated with enzymatic stability and targeted delivery of these molecules that need to be resolved to realize their full potential as emerging drug leads. Here, we have reported the synthesis of an analogue of a naturally occurring short AMP peptide, XLAspP2-RA, in good yield using solid-phase peptide synthesis. The promising anti-proliferative activity of the synthesized peptide together with potent cytotoxicity indicate that XLAspP2-RA may have a significant role in the development of novel anticancer therapeutics. Furthermore, the use of functionalized HNT and GO platforms as stabilizing elements in a com-

posite form significantly improved the enzymatic stability of the peptide. This study provides a promising AMP based strategy for anticancer drug discovery while resolving the remaining issues of peptide-based drug delivery using the tools of nanotechnology.

Declaration of Competing Interest

None.

CRedit authorship contribution statement

Yasuri Amarasekara: Methodology, Validation, Formal analysis, Investigation, Writing – original draft, Visualization. **Inoka C. Perera:** Conceptualization, Methodology, Validation, Resources, Writing – review & editing, Supervision. **Nuwanthi P. Katuwavila:** Conceptualization, Methodology, Validation, Resources, Writing – review & editing, Supervision. **Ranga S. Jayakody:** Resources, Writing – review & editing, Supervision. **Gehan A.J. Amaratunga:** Resources, Writing – review & editing, Supervision. **Laksiri Weerasinghe:** Conceptualization, Methodology, Validation, Resources, Writing – review & editing, Supervision, Project administration, Funding acquisition.

Acknowledgement

This work was funded by the Ministry of Science, Technology, and Research, Sri Lanka (strategic project on graphene oxide).

References

- [1] B.E. Wilson, S. Jacob, M.L. Yap, J. Ferlay, F. Bray, M.B. Barton, Estimates of global chemotherapy demands and corresponding physician workforce requirements for 2018 and 2040: a population-based study, *Lancet Oncol.* 20 (2019) 769–780, doi:10.1016/S1470-2045(19)30163-9.
- [2] IARC biennial report 2020–2021, 2021.
- [3] V. Schirmacher, From chemotherapy to biological therapy: a review of novel concepts to reduce the side effects of systemic cancer treatment (Review), *Int. J. Oncol.* 54 (2019) 407–419, doi:10.3892/ijo.2018.4661.
- [4] J. Harder, R. Gläser, J.M. Schröder, Human antimicrobial proteins - effectors of innate immunity, *J. Endotoxin Res.* 13 (2007) 317–338, doi:10.1177/0968051907088275.

- [5] C. Zhong, L. Zhang, L. Yu, J. Huang, S. Huang, Y. Yao, A review for antimicrobial peptides with anticancer properties: Re-purposing of potential anticancer agents, *BIO Integr.* 1 (2020) 156–167, doi:10.15212/bioi-2020-0013.
- [6] D.W. Hoskin, A. Ramamoorthy, Studies on anticancer activities of antimicrobial peptides, *Biochim. Biophys. Acta Biomembr.* 1778 (2008) 357–375, doi:10.1016/j.bbmem.2007.11.008.
- [7] M. Zasloff, Magainins, a class of antimicrobial peptides from *Xenopus* skin: isolation, characterization of two active forms, and partial cDNA sequence of a precursor, *Proc. Natl. Acad. Sci. U.S.A.* 84 (1987) 5449–5453, doi:10.1073/pnas.84.15.5449.
- [8] R. Anghel, D. Jitaru, L. Bădescu, M. Bădescu, M. Ciocoiu, The cytotoxic effect of magainin II on the MDA-MB-231 and M14K tumour cell lines, *Biomed. Res. Int.* 2013 (2013) 11–13, doi:10.1155/2013/831709.
- [9] S. Liu, H. Yang, L. Wan, H.W. Cai, S.F. Li, Y.P. Li, J.Q. Cheng, X.F. Lu, Enhancement of cytotoxicity of antimicrobial peptide magainin II in tumor cells by bombesin-targeted delivery, *Acta Pharmacol. Sin.* 32 (2011) 79–88, doi:10.1038/aps.2010.162.
- [10] Y. Huan, Q. Kong, H. Mou, H. Yi, Antimicrobial peptides: classification, design, application and research progress in multiple fields, *Front. Microbiol.* 11 (2020) 1–21, doi:10.3389/fmicb.2020.582779.
- [11] L. Huang, D. Chen, L. Wang, C. Lin, C. Ma, X. Xi, T. Chen, C. Shaw, M. Zhou, Dermaseptin-PH: a novel peptide with antimicrobial and anticancer activities from the skin secretion of the south American orange-legged leaf frog, *pithecopus (phylomedusa) hypochondrialis*, *Molecules* (2017) 22, doi:10.3390/molecules22101805.
- [12] L. Huang, D. Chen, L. Wang, C. Lin, C. Ma, X. Xi, T. Chen, C. Shaw, M. Zhou, Dermaseptin-PH: a novel peptide with antimicrobial and anticancer activities from the skin secretion of the south American orange-legged leaf frog, *pithecopus (phylomedusa) hypochondrialis*, *Molecules* (2017) 22, doi:10.3390/molecules22101805.
- [13] A.L. Tornesello, A. Borrelli, L. Buonaguro, F.M. Buonaguro, M.L. Tornesello, Antimicrobial peptides as anticancer agents : functional properties and biological activities, (2020) 1–25.
- [14] A.K. Sato, M. Viswanathan, R.B. Kent, C.R. Wood, Therapeutic peptides : technological advances driving peptides into development, (2006) 638–642, doi:10.1016/j.copbio.2006.10.002.
- [15] C. Pichereau, C. Allary, Therapeutic peptides under the spotlight, *EBR Eur. Biopharm. Rev.* (2005) 88–93.
- [16] C. Release, E. Science, B. Sciences, H. Sciences, Controlled release of macromolecules: biological studies, *J. Controll. Release* 2 (1985) 331–341.
- [17] A.Z. Wang, R. Langer, O.C. Farokhzad, Nanoparticle delivery of cancer drugs, *Annu. Rev. Med.* 63 (2012) 185–198, doi:10.1146/annurev-med-040210-162544.
- [18] Yuko Nakamura, Ai Mochida, Peter Choyke, Hisatake Kobayashi, Nano-drug delivery: is the enhanced permeability and retention (EPR) effect sufficient for curing cancer? *Bioconjugate Chem.* 2016, 27, 10, 2225–2238 27 (10) (2016) 2225–2238, doi:10.1021/acs.bioconjchem.6b00437.
- [19] Mc. Martínez-Ballesta, Á. Gil-Izquierdo, C. García-Viguera, R. Domínguez-Perles, Nanoparticles and controlled delivery for bioactive compounds: outlining challenges for new “smart-foods” for health, *Foods* 7 (2018) 1–29, doi:10.3390/foods7050072.
- [20] Y. Zhang, S. Liu, S. Li, Y. Cheng, L. Nie, G. Wang, C. Lv, W. Wei, C. Cheng, F. Hou, L. Hao, Novel short antimicrobial peptide isolated from *Xenopus laevis* skin, *J. Pept. Sci.* 23 (2017) 403–409, doi:10.1002/psc.2990.
- [21] D. Neubauer, M. Jaśkiewicz, D. Migoń, M. Bauer, K. Sikora, E. Sikorska, E. Kamysz, W. Kamysz, Retro analog concept: comparative study on physicochemical and biological properties of selected antimicrobial peptides, *Amino Acids* 49 (2017) 1755–1771, doi:10.1007/s00726-017-2473-7.
- [22] Y. Amarasekara, Improving the Stability of XLAsp-P2 Through Nano Conjugation, Sri Lanka Institute of Nanotechnology, 2021.
- [23] S. Joshi, R. Siddiqui, P. Sharma, R. Kumar, G. Verma, A. Saini, Green synthesis of peptide functionalized reduced graphene oxide (rGO) nano bioconjugate with enhanced antibacterial activity, *Sci. Rep.* (2020) 1–11, doi:10.1038/s41598-020-66230-3.
- [24] L. Zeraatpishe, A. Mohebal, M. Abdouss, Fabrication and characterization of biocompatible pH responsive halloysite nanotubes grafted with sodium alginate for sustained release of phenytoin sodium, *New J. Chem.* 43 (2019) 10523–10530, doi:10.1039/c9nj00976k.
- [25] R.F. Service, Carbon sheets an atom thick give rise to graphene dreams, *Science* 324 (2009) 875–877, doi:10.1126/science.324.875.
- [26] W.O. Yah, H. Xu, H. Soejima, W. Ma, Y. Lvov, A. Takahara, Biomimetic dopamine derivative for selective polymer modification of halloysite nanotube lumen, *J. Am. Chem. Soc.* 134 (2012) 12134–12137, doi:10.1021/ja303340f.
- [27] P. Yuan, P.D. Southon, Z. Liu, M.E.R. Green, J.M. Hook, S.J. Antill, C.J. Keper, Functionalization of halloysite clay nanotubes by grafting with γ -aminopropyltriethoxysilane, *J. Phys. Chem. C* 112 (2008) 15742–15751, doi:10.1021/jp805657t.
- [28] M. Massaro, G. Cavallaro, C.G. Colletti, G.D. Azzo, S. Guernelli, G. Lazzara, S. Pieraccini, S. RIELA, Halloysite nanotubes for efficient loading, stabilization and controlled release of insulin, *J. Colloid Interface Sci.* (2018), doi:10.1016/j.jcis.2018.04.025.
- [29] M. Massaro, S. RIELA, C. Baiamonte, J.L.J. Blanco, C. Giordano, P. Lo Meo, S. Milioto, R. Noto, F. Parisi, G. Pizzolanti, G. Lazzara, Dual drug-loaded halloysite hybrid-based glycocluster for sustained release of hydrophobic molecules, *RSC Adv.* 6 (2016) 87935–87944, doi:10.1039/C6RA14657K.
- [30] P. Kumarathilaka, V. Jayaweera, H. Wijesekara, I.R.M. Kottegoda, S.R.D. Rosa, M. Vithanage, Insights into starch coated nanozero valent iron-graphene composite for Cr (VI) removal from aqueous medium, 2016 (2016).
- [31] T. Higuchi, Mechanism of sustained-action medication. Theoretical analysis of rate of release of solid drugs dispersed in solid matrices, *J. Pharm. Sci.* 52 (1963) 1145–1149, doi:10.1002/jps.2600521210.
- [32] R.W. Korsemqer, R. Gurny, E. Doelker, P. Buri, N.A. Peppas, Mechanisms of solute release from porous hydrophilic polymers, 15 (1983) 25–35.
- [33] K. Ofori-kwakye, K.A. Mfoafo, S.L. Kipo, N. Kuntworbe, M. El Boakye-gyasi, Development and evaluation of natural gum-based extended release matrix tablets of two model drugs of different water solubilities by direct compression, *Saudi Pharm. J.* (2015), doi:10.1016/j.jsps.2015.03.005.
- [34] H. Jenssen, S.I. Aspomo, Serum stability of peptides, 494 (n.d.) 2022 177–186. 10.1007/978-1-59745-419-3.
- [35] H.A. Cocker, C.R. Pinkerton, L.R. Kelland, Characterization and modulation of drug resistance of human paediatric rhabdomyosarcoma cell lines, *Br. J. Cancer* 83 (2000) 338–345, doi:10.1054/bjoc.2000.1273.
- [36] D. Fernando, A. Adhikari, C. Nanayakkara, E.D. De Silva, R. Wijesundera, Cytotoxic effects of ergone, a compound isolated from *Fulviformes fastuosus*, *BMC Complement. Altern. Med.* (2016) 1–11, doi:10.1186/s12906-016-1471-8.
- [37] T. Barot, D. Rawtani, P. Kulkarni, Heliyon Physicochemical and biological assessment of silver nanoparticles immobilized Halloysite nanotubes-based resin composite for dental applications, *Heliyon* 6 (2020) e03601, doi:10.1016/j.heliyon.2020.e03601.
- [38] Y. Yang, Y. Chen, F. Leng, L. Huang, Z. Wang, W. Tian, Recent advances on surface modification of halloysite nanotubes for multifunctional applications, *Appl. Sci. (Switzerland)* 7 (2017), doi:10.3390/app7121215.
- [39] H. Li, X. Zhu, J. Xu, W. Peng, S. Zhong, Y. Wang, The combination of adsorption by functionalized halloysite nanotubes and encapsulation by polyelectrolyte coatings for sustained drug delivery, *RSC Adv.* 6 (2016) 54463–54470, doi:10.1039/c6ra09599b.
- [40] G.F. Audette, A. Yaseen, N. Bragagnolo, R. Bawa, Protein nanotubes: from bio-nanotech towards medical applications, *Biomedicines* 7 (2019).
- [41] D. Rawtani, G. Pandey, M. Tharmavaram, P. Pathak, Development of a novel 'nanocarrier' system based on Halloysite Nanotubes to overcome the complexation of ciprofloxacin with iron : an *in vitro* approach, *Appl. Clay Sci.* 150 (2017) 293–302, doi:10.1016/j.clay.2017.10.002.
- [42] M. Yan, Nanocomposite for the magnetic separation of proteins, (2017) 30109–30117. 10.1039/c7ra05114j.
- [43] C. Xu, X. Shi, A. Ji, L. Shi, C. Zhou, Y. Cui, Fabrication and characteristics of reduced graphene oxide produced with different green reductants, (2015). 10.1371/journal.pone.0144842.
- [44] S.F. Oliveira, G. Bisker, N.A. Bakh, S.L. Gibbs, M.P. Landry, M.S. Strano, Protein functionalized carbon nanomaterials for biomedical applications, *Carbon* 95 (2015) 767–779, doi:10.1016/j.carbon.2015.08.076.
- [45] H. Wang, Q. Zhang, X. Chu, T. Chen, J. Ge, R. Yu, Graphene oxide – peptide conjugate as an intracellular protease sensor for caspase-3 activation imaging in live cells, (2011) 7065–7069. 10.1002/anie.201101351.
- [46] P. Xing, X. Chu, S. Li, M. Ma, A. Hao, Hybrid gels assembled from Fmoc – amino acid and graphene oxide with controllable properties, (2014) 2377–2385. 10.1002/cphc.201402018.
- [47] C. Ligorio, M. Zhou, J.K. Wychowanec, X. Zhu, C. Bartlam, A.F. Miller, A. Vijayaraghavan, J.A. Hoyland, A. Saiani, Graphene oxide containing self-assembling peptide hybrid hydrogels as a potential 3D injectable cell delivery platform for intervertebral disc repair applications, *Acta Biomater.* 92 (2019) 92–103, doi:10.1016/j.actbio.2019.05.004.
- [48] J. Li, L. Zheng, L. Zeng, Y. Zhang, L. Jiang, J. Song, RGD Peptide-grafted graphene oxide as a new biomimetic nanointerface for impedance-monitoring cell behaviors, 2016 (2016).
- [49] J. Wang, C. Liu, Y. Shuai, X. Cui, L. Nie, Controlled release of anticancer drug using graphene oxide as a drug-binding effector in konjac glucomannan /sodium alginate hydrogels, *Colloids Surf. B Biointerfaces* 113 (2014) 223–229, doi:10.1016/j.colsurfb.2013.09.009.
- [50] D. Depan, J. Shah, R.D.K. Misra, Controlled release of drug from folate-decorated and graphene mediated drug delivery system: synthesis, loading efficiency, and drug release response, *Mater. Sci. Eng. C* 31 (2011) 1305–1312, doi:10.1016/j.msec.2011.04.010.
- [51] J. Jiang, Y. Zhang, D. Cao, P. Jiang, Controlled immobilization of methyltri-oxorhenium (VII) based on SI-ATRP of 4-vinyl pyridine from halloysite nanotubes for epoxidation of soybean oil, *Chem. Eng. J.* 215–216 (2013) 222–226, doi:10.1016/j.cej.2012.03.082.
- [52] D. Tan, P. Yuan, F. Annabi-bergaya, D. Liu, L. Wang, H. Liu, H. He, Loading and *in vitro* release of ibuprofen in tubular halloysite, *Appl. Clay Sci.* (2014) 6–11, doi:10.1016/j.clay.2014.01.018.
- [53] T. Kumeria, M. Bariana, T. Altalhi, M. Kurkuri, C.T. Gibson, W. Yang, D. Losic, Graphene oxide decorated diatom silica particles as new nano-hybrids: towards smart natural drug microcarriers, *J. Mater. Chem. B* 1 (2013) 6302–6311, doi:10.1039/c3tb21051k.
- [54] H. Baishya, Application of mathematical models in drug release kinetics of carbidopa and levodopa ER tablets, *J. Dev. Drugs* 06 (2017) 1–8, doi:10.4172/2329-6631.1000171.
- [55] D.R. Paul, Elaborations on the Higuchi model for drug delivery, *Int. J. Pharm.* 418 (2011) 13–17, doi:10.1016/j.ijpharm.2010.10.037.
- [56] G. Cavallaro, G. Lazzara, S. Milioto, F. Parisi, V. Evtugyn, E. Rozhina, R. Fakhru'llin, Nanohydrogel formation within the Halloysite Lumen for triggered and sustained release, *ACS Appl. Mater. Interfaces* 10 (2018) 8265–8273, doi:10.1021/acsami.7b19361.

- [57] J.H. Petropoulos, K.G. Papadokostaki, M. Sanopoulou, Higuchi's equation and beyond: overview of the formulation and application of a generalized model of drug release from polymeric matrices, *Int. J. Pharm.* 437 (2012) 178–191, doi:[10.1016/j.ijpharm.2012.08.012](https://doi.org/10.1016/j.ijpharm.2012.08.012).
- [58] G. Lavery, Peptide nanomaterials as future antimicrobial technologies, *Future Microbiol.* 13 (2018) 5–7, doi:[10.2217/fmb-2017-0208](https://doi.org/10.2217/fmb-2017-0208).
- [59] L. Di, Strategic approaches to optimizing peptide ADME properties, *AAPS J.* 17 (2015) 134–143, doi:[10.1208/s12248-014-9687-3](https://doi.org/10.1208/s12248-014-9687-3).
- [60] J. Jeroen, S. Smart, H. Franzyk, C. Foged, H. Mørck, Nanoparticle-mediated delivery of the antimicrobial peptide plectasin against *Staphylococcus aureus* in infected epithelial cells, *Eur. J. Pharm. Biopharm.* (2015), doi:[10.1016/j.ejpb.2015.02.009](https://doi.org/10.1016/j.ejpb.2015.02.009).
- [61] A. Brill, A. Torchinsky, H. Carp, V. Toder, The role of apoptosis in normal and abnormal embryonic development, *J. Assist. Reprod. Genet.* 16 (1999) 512–519, doi:[10.1023/A:1020541019347](https://doi.org/10.1023/A:1020541019347).
- [62] C. Bézivin, S. Tomasi, F.L. Dévéhat, J. Boustie, Cytotoxic activity of some lichen extracts on murine and human cancer cell lines, (2003) 499–503.
- [63] P. Prayong, S. Barusrux, N. Weerapreeyakul, Cytotoxic activity screening of some indigenous Thai plants cytotoxic activity screening of some indigenous Thai plants, *Fitoterapia* 79 (2020) 598–601, doi:[10.1016/j.fitote.2008.06.007](https://doi.org/10.1016/j.fitote.2008.06.007).